Numerical Investigation of Al-Reinforced CFRP Composite under Low-Velocity Impact

Maria Pia Falaschetti[1,a*], Nicola Zavatta[2,b], Francesco Rondina[3,c], Lorenzo Donati[3,d] and Enrico Troiani[3,e]

[1*]Interdepartmental Centre for Industrial Research on Advanced Applications in Mechanical Engineering and Materials Technology, CIRI-MAM, University of Bologna, Viale Risorgimento 2, 40136 Bologna, Italy

[2]Interdepartmental Centre for Industrial Research on Aerospace, CIRI-Aerospace, University of Bologna, Via Fontanelle 40, 47121 Forlì, Italy

[3]University of Bologna, Department of Industrial Engineering DIN, Via Fontanelle 40, 47121 Forlì, Italy

[a*]mariapi.falaschetti2@unibo.it, [b]nicola.zavatta2@unibo.it, [c]francesco.rondina2@unibo.it, [d]l.donati@unibo.it, [e]enrico.troiani@unibo.it

Abstract. Fibre-reinforced composite materials are widespread in lightweight, high-performance applications. However, polymeric composites generally exhibit a brittle behaviour, which makes them susceptible to impact damage. Even low-velocity impacts can produce delaminations, which cause a substantial reduction of the compressive mechanical properties. Metallic layers have been embedded in composite laminates with the aim to improve their fracture behaviour: aluminium plies can be employed to increase the indentation resistance of Carbon Fibre Reinforced Polymers (CFRP) specimens. For this reason, hybrid fibre-metal laminates are expected to be a viable solution to reduce the damage caused by low-velocity impacts.

In this work, CFRP specimens reinforced with aluminium plies were modelled using the finite element method and a cohesive zone model. Cohesive elements based on a traction-separation formulation were embedded at each ply-to-ply interface to enforce delamination damage. Different configurations of the Al reinforcements were studied by varying the position of the aluminium layers between the CFRP plies.

Introduction

Fibre-reinforced composite materials are widely employed in the industry due to their good properties and the possibility to create ad-hoc materials for specific loading conditions. Due to their advantageous strength-to-weight ratio, Carbon Fibre Reinforced Plastics (CFRP) are widely used in the aeronautic and automotive industries. Nevertheless, the complexity of the fracture mechanics analysis and, therefore, of the prediction of the material behaviour in operative conditions, have hindered the possible enhancements given by these materials. In fact, due to their inhomogeneity, it is not possible to reliably foresee how a flaw inside a composite could influence its operative life; moreover, the possibility of unexpected events (e.g. impacts) could lead to a sudden failure. All these uncertainties lead to rigid regulations [1,2] which heavily limit the benefits of composite materials.

In the aeronautical or automotive industry, impacts on composite structures are not infrequent. In 1988 a study [3] regarding necessary repairs on 71 aircraft Boeing 747, operating in 17 different countries and with an average life of 29500 flight hours, was conducted. 688 fatigue, corrosion, and impact damage sites were detected during maintenance inspections and repaired. From the analysis of primary structures only, 396 fatigue cracks (57.6%), 202 corrosion defects (29.4%) and 90 impact damage spots (13.0%) were found. More recently, a similar study conducted on the Airbus A320 family has shown that impacts cannot be neglected [4].

Based on the impact velocity, impacts can be categorised [5,6] in: low-velocity (up to 10 m/s), intermediate velocity (between 10 and 50 m/s), high-velocity (comprised between 50 and 1000 m/s) and hypervelocity (greater than 2 km/s) impacts. Low-velocity impacts are usually due to tool drops during maintenance or to luggage loading operations. These, as well as intermediate velocity impacts (caused for example by running debris on the landing strip), are the most common. These kinds of impacts could generate intra-laminar delaminations or other internal defects without any or negligible evidence on the external surface, being therefore referred as Barely Visible Impact Damage (BVID). Moreover, it has been demonstrated [7,8] that low energy impact can result in a compressive residual strength drop of around 10% when the impact occurs in the centre of the specimen, and around 30% when there is a near-edge impact (i.e. an impact close to the component border). This strength reduction, combined with the absence of visible defects, could lead to a dangerous unexpected failure.

In order to overcome composite drawbacks, Fibre Metal Laminates (FML) have been developed. These laminates are hybrid materials that combine advantages of both composite and metallic materials, in particular plasticity for the metal and high fatigue life for composites [9–11]. Some studies have been done related to standard FML impact behaviour [12,13]. However, little investigation has been carried out on the effect of metal layers position inside a fibre-metal laminate.

Due to the complexity of the impact event and its effects on composite materials, adopting only an experimental approach for the design of a composite component is usually highly time-consuming and quite expensive. For this reason, numerical analysis can be employed to speed up the design process. Since the advent of Finite Element Method (FEM) analysis, many different models regarding material damage have been developed. Among them, Continuum Damage Mechanics (CDM) is largely implemented for progressive damage analysis. In the CDM approach, the effects of damage are considered by degrading the material properties by means of damage variables [14,15]. The CDM model was originally implemented in the '60s and is widely applied for matrix and fibre 'in-ply' damage in composite models. However, under impact loading, in particular low energies impact, delamination is the most common failure mode. In order to model this kind of damage, Cohesive Zone Model (CZM) [16–18] is usually effectively implemented.

In this paper, four different FML stacking sequences are compared aiming to find the best configuration. Laminates were tested through numerical analysis (by means of Abaqus software, and well know, and validated, damage models): solid carbon/epoxy laminate without aluminium layers (12C configuration), aluminium layers located in the outer surfaces (ALE configuration), aluminium sheets in the centre of the specimen (glued together by means of epoxy resin, ALM configuration) and Al layers in an intermediate position between the external surface and the specimen mid-plane (ALW configuration).

Material and Methods

The FEM model was implemented in Abaqus software. In the following section, the damage models used are briefly described.

Composite damage. The damage initiation for composite plies is based on Hashin's theory [19], that consists of four different initiation mechanisms:

Fibre tension ($\sigma_{11} \geq 0$)
$$F_f^T = \left(\frac{\sigma_{11}}{X^T}\right)^2 + \alpha\left(\frac{\tau_{12}}{S^L}\right)^2 \tag{1}$$

Fibre compression ($\sigma_{11} < 0$)
$$F_f^C = \left(\frac{\sigma_{11}}{X^C}\right)^2 \tag{2}$$

Matrix tension ($\sigma_{22} \geq 0$)
$$F_m^T = \left(\frac{\sigma_{22}}{Y^T}\right)^2 + \left(\frac{\tau_{12}}{S^L}\right)^2 \tag{3}$$

Matrix compression ($\sigma_{22} < 0$)
$$F_m^C = \left(\frac{\sigma_{22}}{2S^T}\right)^2 + \left[\left(\frac{Y^C}{2S^T}\right)^2 - 1\right]\frac{\sigma_{22}}{Y^C} + \left(\frac{\tau_{12}}{S^L}\right)^2 \tag{4}$$

where F is the critical damage parameter, X^T and X^C are the longitudinal tensile and compressive strength respectively, Y^T and Y^C are the transverse tensile and compressive strength respectively, S^L and S^T the longitudinal and the transverse shear strength, α a coefficient to account for the shear stress contribution to fibre tensile initiation criterion and σ_{11}, σ_{22} and τ_{12} are the components of the effective stress tensor (longitudinal stress, transversal stress and shear stress, respectively).

Cohesive elements. Cohesive layers were modelled by means of the cohesive elements implemented in Abaqus software (COH3D8). These elements were used to model interlaminar resin-rich areas using a traction-separation law and a quadratic nominal stress damage criterion (QUADS).

The traction-separation law is defined by a function between traction force and displacement. A linear elastic behaviour is assumed before the damage onset (defined by the cohesive strength and the characteristic length). This can be defined as:

$$\sigma = \begin{bmatrix} \sigma_n \\ \sigma_s \\ \sigma_t \end{bmatrix} = \begin{bmatrix} K_{nn} & K_{ns} & K_{nt} \\ K_{ns} & K_{ss} & K_{st} \\ K_{nt} & K_{st} & K_{tt} \end{bmatrix} \begin{bmatrix} \varepsilon_n \\ \varepsilon_s \\ \varepsilon_t \end{bmatrix} = \boldsymbol{K}\varepsilon \tag{5}$$

where σ is the stress vector composed by the normal (σ_n) and shear components (σ_s, σ_t), the matrix $\boldsymbol{K}$ is composed by the elastic modulus components and ε is the nominal strain vector. The relationship between strain and displacement is given by:

$$\varepsilon_n = \frac{\delta_n}{T} \quad ; \quad \varepsilon_s = \frac{\delta_s}{T} \quad ; \quad \varepsilon_t = \frac{\delta_t}{T} \tag{6}$$

where T is the thickness of the cohesive elements (that was assumed equal to 1). After the damage onset, a damage evolution function has to be defined, reproducing the cohesive softening due to the failure. A quadratic nominal stress (QUADS) criterion was implemented, defined as:

$$\left\{ \frac{\langle \sigma_n \rangle}{\sigma_n^0} \right\}^2 + \left\{ \frac{\sigma_s}{\sigma_s^0} \right\}^2 + \left\{ \frac{\sigma_t}{\sigma_t^0} \right\}^2 = 1 \tag{8}$$

where the Macaulay bracket, $<\ >$, signifies that the compressive stress does not contribute to damage initiation, σ_n^0, σ_s^0 and σ_t^0 are the peak values of the nominal stress along a direction normal to the interface and along the first and second shear direction, respectively. Beyond the damage onset, material softening is defined by parameter D:

$$\sigma_D = (1-D)\boldsymbol{K}\epsilon = (1-D)\sigma \qquad 0 \leq D \leq 1 \tag{9}$$

The damage evolution can be defined based on the energy dissipated due to damage. The components of fracture energy are implemented as material properties and the equivalent fracture energy under mixed mode conditions is computed following Benzeggagh-Kenane (BK) model [20]. It can be described as:

$$G_C = G_{IC} + (G_{IIC} - G_{IC})\left(\frac{G_{II} + G_{III}}{G_I + G_{II} + G_{III}} \right)^{\eta} \tag{10}$$

where G_C is the critical strain energy release rate, G_{IC} and G_{IIC} are the fracture toughness for mode I and II, G_I, G_{II} and G_{III} the energy release rates in mode I, II and III, and η is the BK material coupling parameter.

Model characteristics. The materials selected for this study are Al2024-T3 aluminium plates and G939 Fabric/HexPly M18/1 plane weave fabric carbon/epoxy plies. In the numerical model, the

aluminium sheets and the composite plies have a thickness of 0.4 mm and 0.227 mm respectively. The mechanical properties of the two materials are listed in Table 1 to 4; for the aluminium material model, plasticity with isotropic hardening is implemented.

Table 1: Composite properties

Property	Value
ρ	1.72 g/cm^3
X^T, X^C	800 MPa
Y^T, Y^C	800 MPa
S^L, S^T	100 MPa
E_{11}	65 GPa
E_{22}	65 GPa
G_{12}, G_{23}, G_{13}	3.9 GPa
ν_{12}	0.32

Table 2: Cohesive properties

Property	Value
ρ	1.22 g/cm^3
σ_n^0	50 MPa
σ_s^0	30 MPa
σ_t^0	30 MPa
K_{nn}	780 GPa/mm
K_{ss}	390 GPa/mm
K_{tt}	390 GPa/mm
G_{Ic}	280 J/m^2
G_{IIc}	790 J/m^2
G_{IIIc}	790 J/m^2

Table 3: Aluminium properties

Property	Value
ρ	2.92 g/cm^3
σ_{11}	345 MPa
E_{11}	68.7 GPa
ν	0.35

Table 4: Aluminium plasticity curve

Stress [MPa]	Plastic strain [-]
345	0
440	0.05
475	0.10
483	0.15

Specimens geometry was based on [7] and therefore the specimens were 140 mm long and 30 mm wide. The thickness of each model was different, according to the implemented configurations. The four configurations were:

- 12C (Figure 1-a): made of 12 plane weave carbon/epoxy plies $[(0/90)_f]_{6s}$
- ALE (Figure 1-b): 8 plain weave carbon/epoxy plies, 2 aluminium layers in the external surfaces $[Al/(0/90)_{f_4}]_s$
- ALW (Figure 1-c): 8 plain weave carbon/epoxy plies, 2 aluminium layers as $[(0/90)_{f_2}/Al/(0/90)_{f_2}]_s$
- ALM (Figure 1-d): 8 plain weave carbon/epoxy plies, 2 aluminium layers as $[(0/90)_{f_4}/Al/\overline{resin}]_s$

Composite plies are modelled with continuum shell elements (SC8R), while aluminium layers are modelled with 3D deformable elements (C3D8R). In both cases, elements are 1 mm long near the impact region. In order to achieve similar element dimension, the composite plies were discretised with one layer through the thickness, while the Al sheet were meshed with two layers. Cohesive layers of 0.01 mm thickness are discretised with 3D elements (COH3D8) of 0.5 mm lateral dimension in the impact area. The impactor was modelled as a hemispherical discrete rigid body (R3D4), having a mass of 1.7 kg concentrated in the centre of gravity node. In all models, the impact energy was set equal to 5 J, based on [7,8].
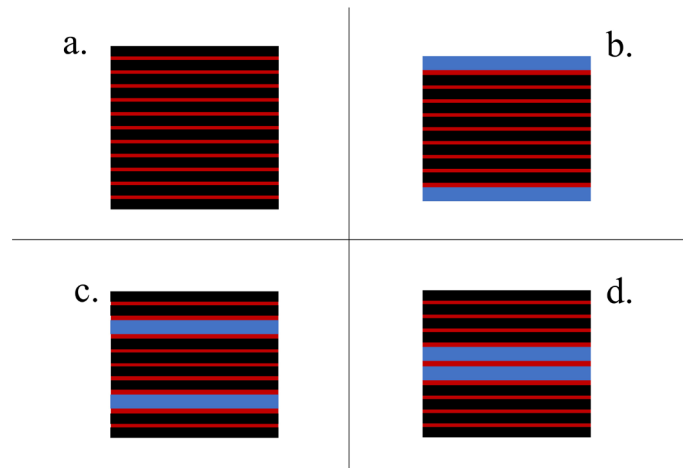
Figure 1: Modelled stacking sequences (composite plies in black, aluminium layers in blue, cohesive layers in red).

Thanks to the symmetry, only a quarter of the configuration was modelled to reduce computational time. Proper boundary conditions were used along the symmetry planes. The models, therefore, resulted to be 15 mm wide and 70 mm long. The impactor was constrained to move only along the direction orthogonal to the specimen plane, whilst the 15 mm steel clamping fixture at one end was modelled by constraining the displacements degrees of freedom. Different plies were connected using tie constraints. Concurrently, non-penetration contacts were defined between adjacent composite plies, as well as between the impactor and the external surface of the specimen. Different friction coefficients were used: 0.5 between composite pairs and 0.3 between impactor and the first prepreg layer [21].

Results and discussion

The results for the four models are here compared and discussed. Figure 2-Figure 5 show the damage in the cohesive layers: the layers have been numbered in descending order starting from the layer closer to the impactor to the one on the opposite side. It is possible to notice that the delaminated areas, shown in grey, are slightly smaller in the hybrid coupons, in particular in the ALE specimen.

In all models, the delamination area is roughly rounded, exhibiting the usual behaviour of the delamination failure mode growing along the direction of fibre orientation of the adjacent plies [5]. In this case, the area is rounded due to the composite fabric. Moreover, a stressed (not yet damaged) area close to the fixed end can be spotted. This area is wider, and the damage variable is slightly higher, in the 12C and ALM models whilst it gets smaller in ALW and ALE. In the latter, the damage parameter value is the lowest. Therefore, placing aluminium layers in, or close to, the external surfaces results in a smoother distribution of the stress concentration.

In Figure 6 the impact energy is shown. The influence of the laminate stacking sequence can be observed: while ALM, ALW and 12C models have a quite similar behaviour due to the presence of the composite on the external layers, ALE model has a lower rebound energy. The higher absorbed energy of the ALE case (Table 5) can be justified by the plastic deformation of the external aluminium layer highlighted in Figure 7. This plastic deformation is not observed in ALM and ALW model. The aluminium on the external surfaces of the specimen has an influence on the impact force as well: as it can be observed from Figure 8, the closer the position of the Al layer to the impactor, the lower is the amplitude of the force oscillations. In fact, the impact force curve of the ALE model has a smoother behaviour compared to those of the other models.
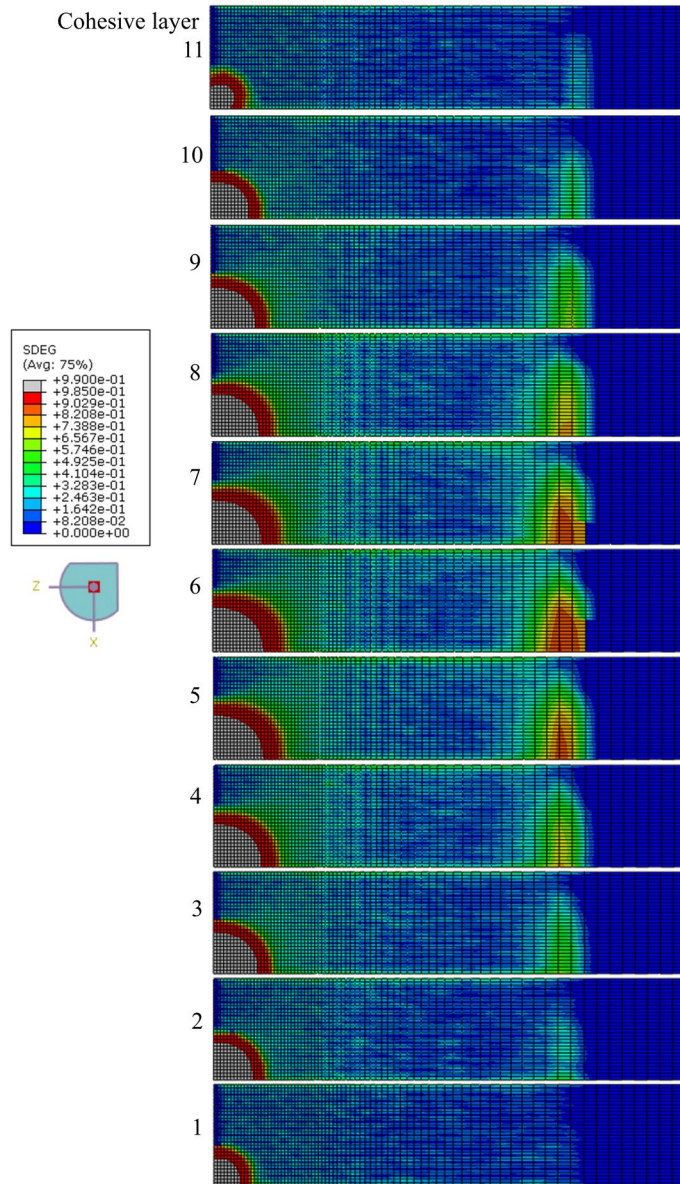
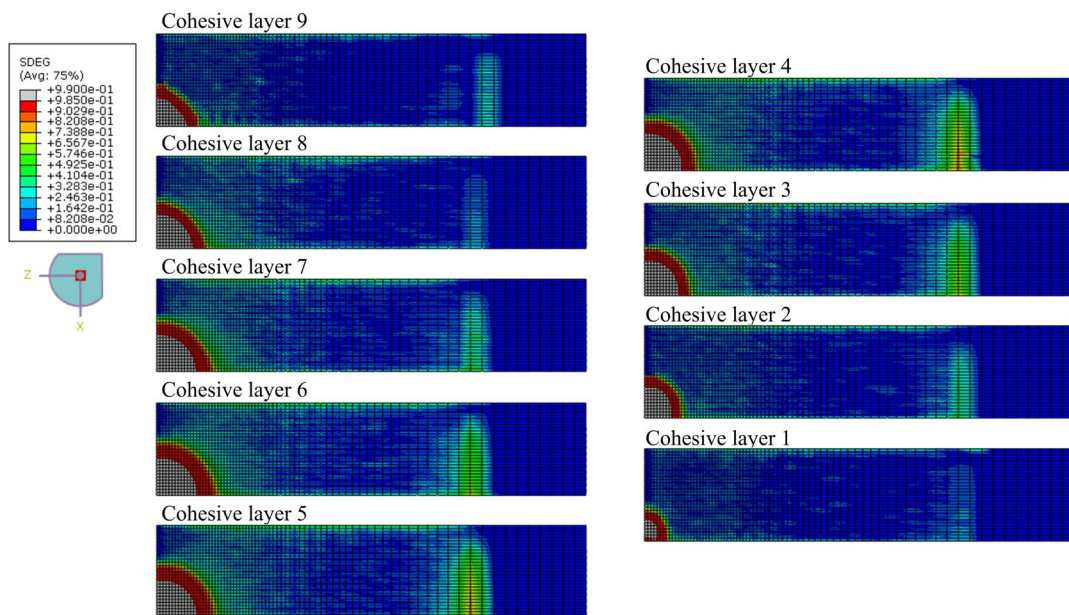Figure 2: 12C model cohesive layers, damage parameter.

Figure 3: ALE model cohesive layers, damage parameter.

An estimated value of the damaged area, for the most damaged cohesive layers per each model, is listed in Table 5. This is higher for the 12C and ALW models whilst it decreases in ALM and ALE models, showing the lowest value in the latter case.
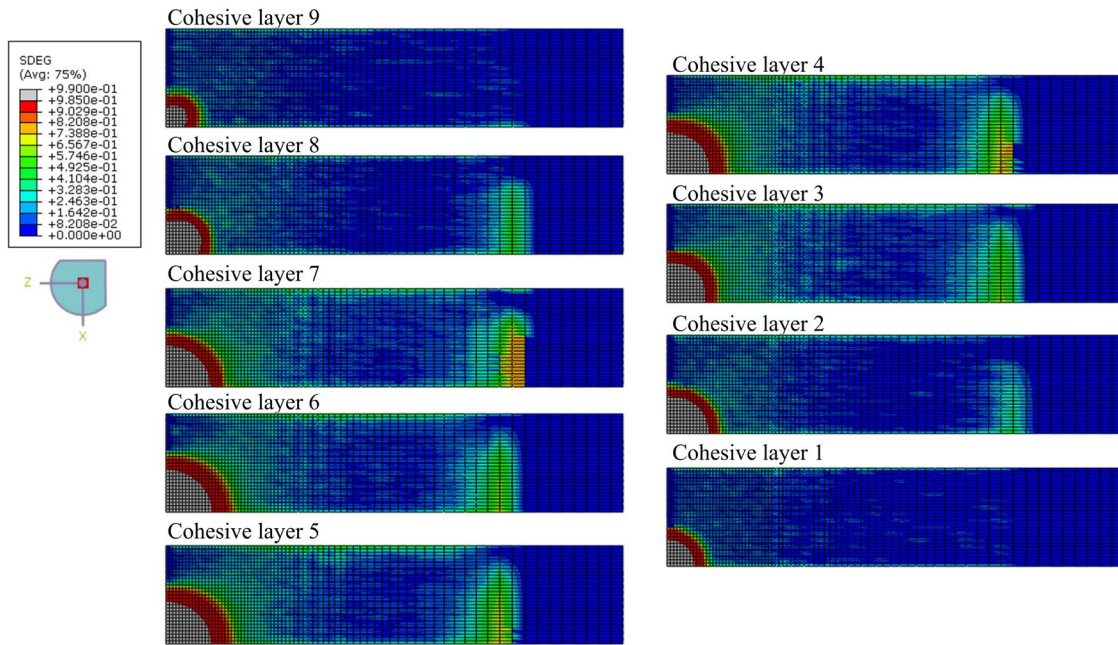

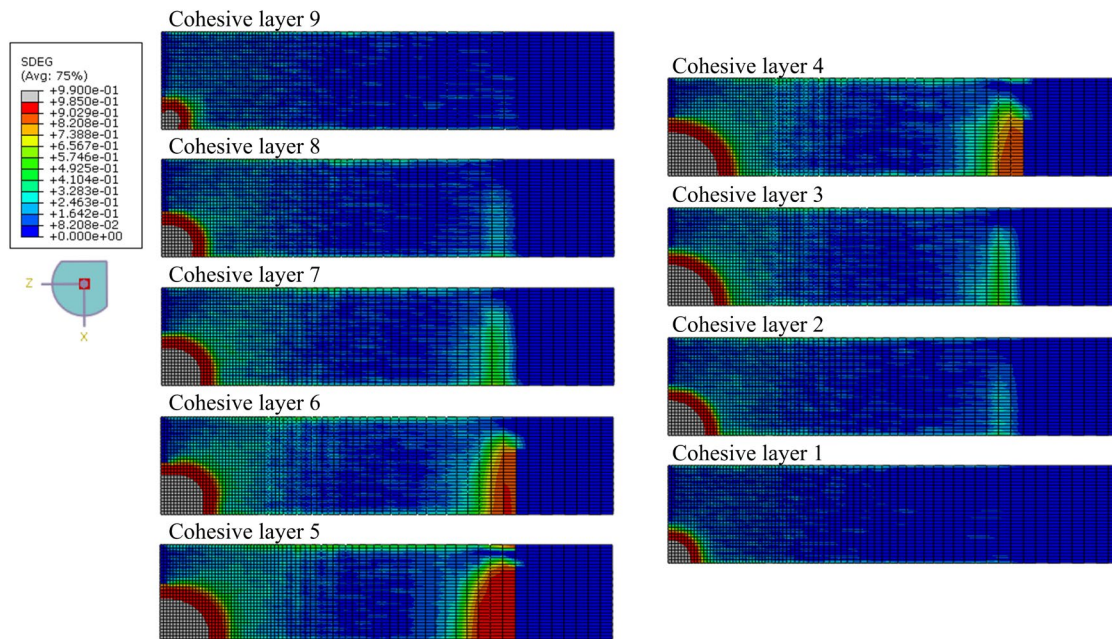Figure 4: ALW model cohesive layers, damage parameter.

Figure 5: ALM model cohesive layers, damage parameter.

Table 5: Main results of the simulations – values.

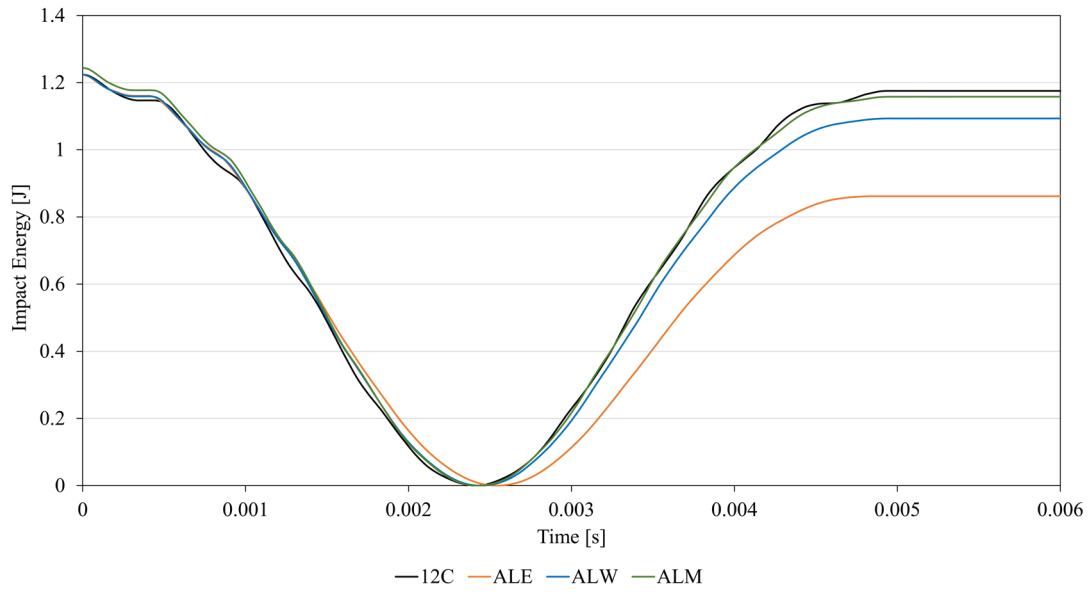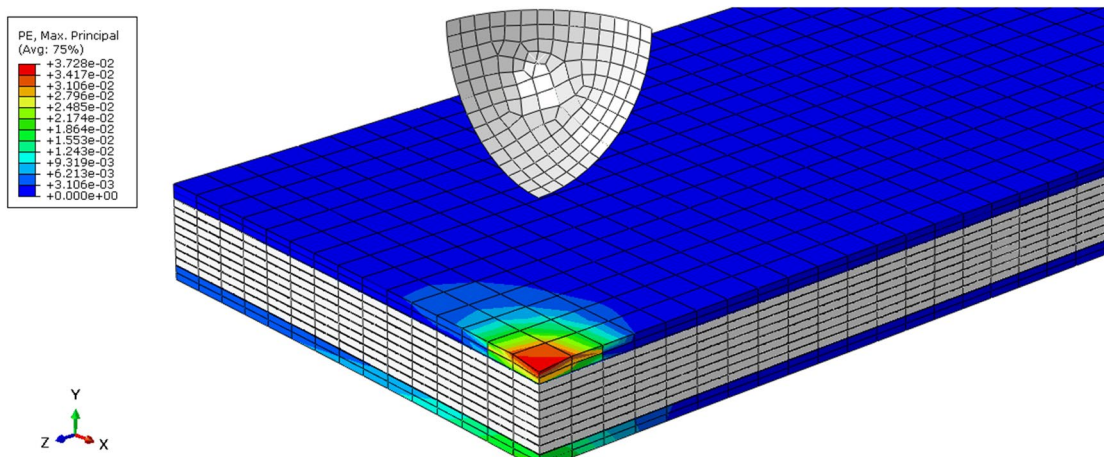|	Max Displacement [mm]	Max Contact Force [N]	Rebound Velocity [mm/s]	Absorbed Energy [J]	Max delaminated area (appr.) [mm^2]
12C	-3.88	-868	2351	0.05	38.48
ALE	-4.04	-721	2013	0.36	33.18
ALW	-3.94	-802	2268	0.13	38.48
ALM	-3.96	-836	2334	0.07	35.78

Figure 6: Impact energy.

Figure 7: Residual strain in the Al layers in ALE model (composite layers and impactor are in white).
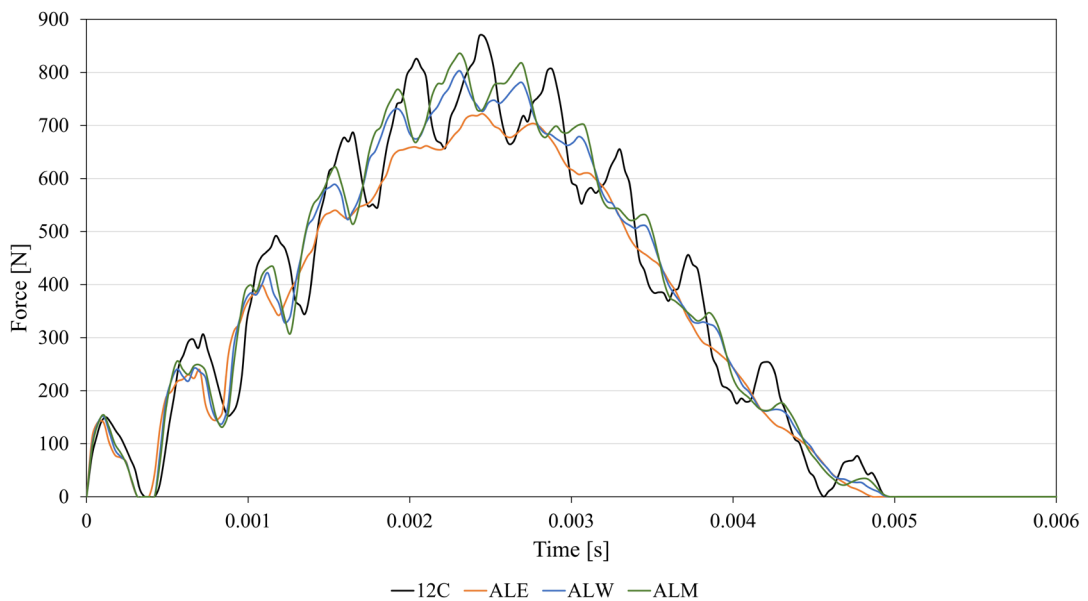

Figure 8: Contact force.

By plotting the Hashin's failure parameter near the impact location (Figure 9), the extension of the area affected by fibre damage can be evaluated. Coupons with composite layers on the outside show a damaged area that is extended to the lower plies, down to the first aluminium sheet; below the first aluminium layer, no damage is observed. When the aluminium layer is placed at the external surface (ALE model), the damage of the composite plies is effectively suppressed throughout the thickness of the laminate.
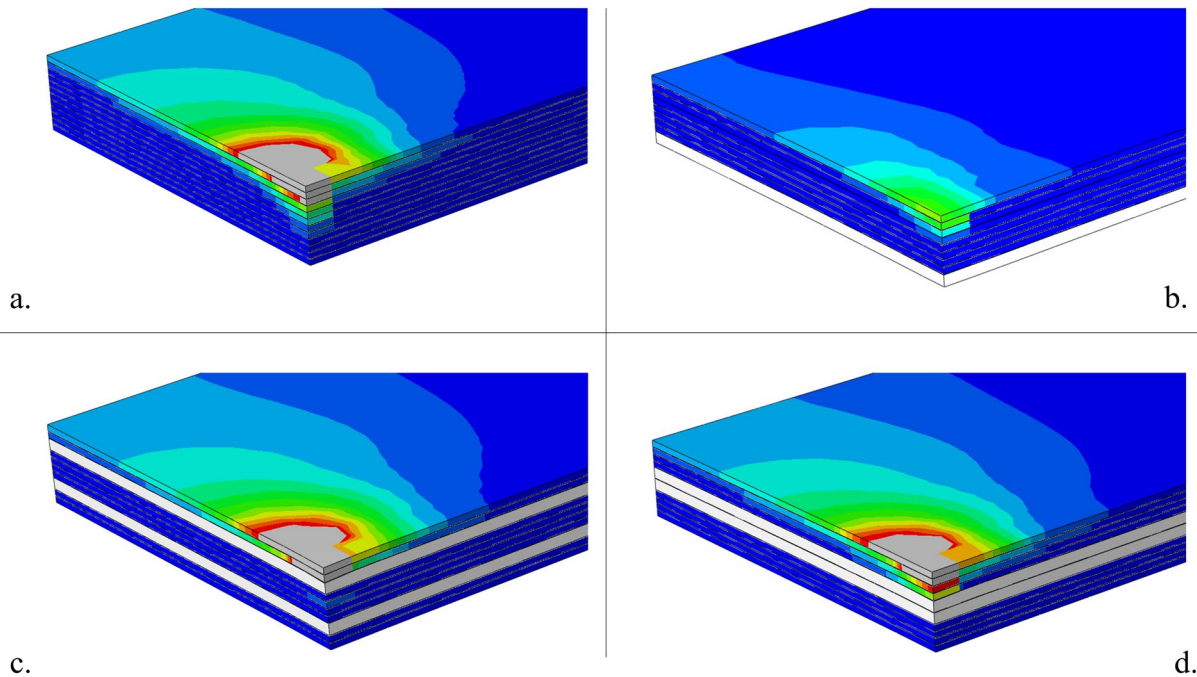

Figure 9: Fibre compression damage parameter F_f^C: a. 12C, b. ALE (first aluminium layers is hidden), c. ALW, d. ALM). Aluminium sheets are in white. The damaged area, i.e. region where damage exceeds 1, is shown in grey.

Conclusions

In this paper, a numerical comparison between specimens with different fibre-metal stacking sequences was described. The models represented the phenomenon of a low energy impact on a flat composite structure, a frequent event in the aeronautic field that could result in inner damage and, consequently, influence the material residual strength. The implemented stacking sequences were composed of carbon/epoxy fabric prepreg plies and aluminium layers. The aim was to identify the optimal position of the aluminium layers within the laminates, such that the extent of the impact damage is minimized. Although further analyses are needed to verify the sensitivity of the models to numerical parameters (e.g. mesh size), it was observed that having aluminium sheets in the outer surface could represent the best configuration: interlaminar damage is smaller despite the higher absorbed energy and the inner composite layers are free from damage. Additionally, due to plasticisation of the aluminium, a permanent deformation can be spotted even for a low impact energy. This could facilitate the impact damage detection during maintenance operations, helping in identifying low energy impact locations even during the first bare-eye inspection.

References

[1]   FAA. AC 20-107A: Composite Aircraft Structure. vol. 1. 2010.

[2]   FAA. AC 20-107B: Composite Aircraft Structure. vol. 1. 2010.

[3]   Vlot A. Low-velocity impact loading: On fibre reinforced aluminium laminates (ARALL and GLARE) and other aircraft sheet materials. Delft: Delft University of Technology; 1993.

[4]   Airbus Magazine Fast 48 2011.

[5]   Abrate S. Impact on laminated composite materials. Appl Mech Rev 1991;44:155–90. https://doi.org/10.1115/1.3119500.

[6]   Abrate S. Impact on laminated composites: Recent advances. Appl Mech Rev 1994;47:517–44. https://doi.org/10.1115/1.3111065.

[7]   Falaschetti MP, Scafè M, Troiani E, Agostinelli V, Sangiorgi S. Experimental Determination of Compressive Residual Strength of a Carbon/epoxy Laminate after a Near-edge Impact. Procedia Eng., vol. 109, Elsevier Ltd; 2015, p. 171–80. https://doi.org/10.1016/j.proeng.2015.06.229.

[8]   Falaschetti MP, Scafè M, Tatì A, Troiani E. Experimental determination of thickness influence on compressive residual strength of impacted carbon/epoxy laminate. Procedia Struct. Integr., vol. 3, Elsevier B.V.; 2017, p. 237–45. https://doi.org/10.1016/j.prostr.2017.04.056.

[9]   Asundi A, Choi AYN. Fiber metal laminates: An advanced material for future aircraft. J Mater Process Technol 1997;63:384–94. https://doi.org/10.1016/S0924-0136(96)02652-0.

[10]   Laliberte J, Poon C, Straznicky PV, Fahr A. Applications of fiber-metal laminates. Polym Compos 2000;21:558–67.

[11]   Krishnakumar S. Fiber Metal Laminates — The Synthesis of Metals and Composites. Http://DxDoiOrg/101080/10426919408934905   2007;9:295–354. https://doi.org/10.1080/10426919408934905.

[12]   Sadighi M, Alderliesten RC, Benedictus R. Impact resistance of fiber-metal laminates: A review. Int J Impact Eng 2012;49:77–90. https://doi.org/10.1016/J.IJIMPENG.2012.05.006.

[13]   Sadighi M, Pärnänen T, Alderliesten RC, Sayeaftabi M, Benedictus R. Experimental and Numerical Investigation of Metal Type and Thickness Effects on the Impact Resistance of Fiber Metal Laminates n.d. https://doi.org/10.1007/s10443-011-9235-6.

[14]   Chaboche JL. Continuum Damage Mechanics: Part I—General Concepts. J Appl Mech 1988;55:59–64. https://doi.org/10.1115/1.3173661.

[15]   Chaboche JL. Continuum Damage Mechanics: Part II—Damage Growth, Crack Initiation, and Crack Growth. J Appl Mech 1988;55:65–72. https://doi.org/10.1115/1.3173662.

[16]   Camanho PP, Dávila CG. Mixed-Mode Decohesion Finite Elements for the Simulation of Delamination in Composite Materials. 2002.

[17]   Faggiani A, Falzon BG. Predicting low-velocity impact damage on a stiffened composite panel n.d. https://doi.org/10.1016/j.compositesa.2010.02.005.

[18]   Johnson HE, Louca LA, Mouring S, Fallah AS. Modelling impact damage in marine composite panels q 2008. https://doi.org/10.1016/j.ijimpeng.2008.01.013.

[19]   Hashin Z. Failure criteria for unidirectional fiber composites. J Appl Mech Trans ASME 1980;47:329–34. https://doi.org/10.1115/1.3153664.

[20]   Benzeggagh ML, Kenane M. Measurement of mixed-mode delamination fracture toughness of unidirectional glass/epoxy composites with mixed-mode bending apparatus. Compos Sci Technol 1996;56:439–49. https://doi.org/10.1016/0266-3538(96)00005-X.

[21]   Shi Y, Swait T, Soutis C. Modelling damage evolution in composite laminates subjected to low velocity impact. Compos Struct 2012; 94: 2902–13. https://doi.org/10.1016/j.compstruct.2012.03.039.